PROTEINS: Structure, Function, and Bioinformatics 68:503–515 (2007)

pyDock: Electrostatics and Desolvation for Effective Scoring of Rigid-Body Protein–Protein Docking

Tammy Man-Kuang Cheng,[1] Tom L. Blundell,[1] and Juan Fernandez-Recio[2,3]*

[1]*Department of Biochemistry, University of Cambridge, Cambridge CB2 1GA, United Kingdom*
[2]*Structural and Computational Biology Department, Institute for Research in Biomedicine, C/ Josep Samitier 1-5, E-08028 Barcelona, Spain*
[3]*Department of Life Sciences, Barcelona Supercomputing Center, C/ Jordi Girona 29, E-08034 Barcelona, Spain*

ABSTRACT **The accurate scoring of rigid-body docking orientations represents one of the major difficulties in protein–protein docking prediction. Other challenges are the development of faster and more efficient sampling methods and the introduction of receptor and ligand flexibility during simulations. Overall, good discrimination of near-native docking poses from the very early stages of rigid-body protein docking is essential step before applying more costly interface refinement to the correct docking solutions. Here we explore a simple approach to scoring of rigid-body docking poses, which has been implemented in a program called pyDock. The scheme is based on Coulombic electrostatics with distance dependent dielectric constant, and implicit desolvation energy with atomic solvation parameters previously adjusted for rigid-body protein–protein docking. This scoring function is not highly dependent on specific geometry of the docking poses and therefore can be used in rigid-body docking sets generated by a variety of methods. We have tested the procedure in a large benchmark set of 80 unbound docking cases. The method is able to detect a near-native solution from 12,000 docking poses and place it within the 100 lowest-energy docking solutions in 56% of the cases, in a completely unrestricted manner and without any other additional information. More specifically, a near-native solution will lie within the top 20 solutions in 37% of the cases. The simplicity of the approach allows for a better understanding of the physical principles behind protein–protein association, and provides a fast tool for the evaluation of large sets of rigid-body docking poses in search of the near-native orientation. Proteins 2007;68: 503–515.** **© 2007 Wiley-Liss, Inc.**

Key words: protein–protein association; rigid-body docking; CAPRI; ASA-based desolvation; atomic solvation parameter; binding energy

INTRODUCTION

Most of biological functions in living organisms involve the formation of transient or permanent specific protein–protein complexes. A detailed structural knowledge of such complexes is essential for a proper understanding of molecular biology processes at atomic resolution, and also to map complex protein interaction networks and macromolecular assemblies,[1,2] with the ultimate goal of being able to interfere with processes of therapeutical or biotechnological interest. However, structural information at atomic resolution on protein–protein complexes is less extensive than that on unbound proteins. Therefore there is an increasing need for computational tools that can model and analyze protein–protein interactions at atomic resolution. Given the high interest in this, a number of computational docking algorithms have been described that aim to predict the structure of a protein–protein complex from their individual subunits.[3–5]

The recent CAPRI experiments (http://capri.ebi.ac.uk) provide an assessment of the successes and limitations of current docking methods.[6,7] They nicely identify the major challenges in protein–protein docking prediction as: (i) accurate scoring of rigid-body docking orientations; (ii) development of faster and more efficient sampling methods; and (iii) treatment of receptor and ligand flexibility during simulations. Good discrimination of near-native docking poses from the very early stages of protein docking (which usually deal with rigid-body geometries) is required before applying more costly interface refinement to the correct rigid-body docking solutions.

There are different approaches for the sampling and scoring of the mutual orientations of the two interacting molecules. Many well-known docking methods are using a grid-based 3D representation of the proteins and aim to identify the best correlation between the two grids. Translating the grids over *xyz* coordinates can be dramatically sped up by using Fast Fourier Transform (FFT) algorithms. These docking methods, such as GRAMM,[8] DOT,[9] MolFit,[10] FTDOCK,[11] ZDOCK,[12] or

Grant sponsor: Marie Curie European Reintegration (EC); Grant sponsor: Ministerio de Educación y Ciencia, Spain; Grant number: BIO2004-05879.

*Correspondence to: Dr. Juan Fernandez-Recio, Department of Life Sciences, Barcelona Supercomputing Center, C/ Jordi Girona 29, E-08034 Barcelona, Spain. E-mail: juan.fernandez@bsc.es

Received 13 November 2006; Revised 8 January 2007; Accepted 15 January 2007

Published online 19 April 2007 in Wiley InterScience (www.interscience.wiley.com). DOI: 10.1002/prot.21419

BiGGER,[13] provide a good spatial sampling at low computational cost, but the limitations of the rigid-body approach and the simple grid representation make difficult to get docking poses geometrically accurate. HEX[14] is an alternative method that uses polar Fourier correlations to accelerate docking calculations. On the other side, methods based on global-energy optimization, such as RosettaDock,[15] ICM-DISCO,[16] or HADDOCK,[17] aim to search for the energy minima in the vicinity the complex state, including terms for van der Waals contacts, electrostatics, hydrogen-bonding and desolvation. Even when using rigid-body or pseudo rigid-body (some parts of the protein are flexible) approaches, they can provide reasonable geometries, as the scoring functions can be adjusted to be less dependent on the possible geometrical inaccuracies of the interfaces.

One of the reported docking methods based on global-energy optimization, ICM-DISCO consisted of a first step based on Monte–Carlo sampling of rigid-body orientations, followed by scoring of resulting docking poses by the initial scoring function plus the ASA-based solvation energy, and finally a last step based on refinement of the ligand interface side-chains by a Biased-Probability Monte–Carlo sampling.[16] This scheme gave excellent results not only for internal benchmarks,[16] but also for external blind tests as the first rounds of CAPRI.[6,18] The refinement step proved to be very helpful in some cases, but the bottle-neck was clearly the discrimination of good orientations amongst the thousands of rigid-body docking poses during the first step. The ASA-based desolvation energy, with atomic solvation parameters optimized for rigid-body protein–protein docking, improved dramatically the predictive results of the ICM scoring function.[19] This scoring function together with an efficient clustering of near-native docking orientations was used for accurate prediction of protein-binding sites,[19] and yielded good models in almost 90% of the targets of the last CAPRI round.[7,20] The main problem with this approach is the computational cost of sampling a large number of docking poses by the Monte–Carlo procedure to exhaustively explore the docking energy landscape.

In the present work we analyze the essential aspects of this scoring function, and explore whether it can be applied to other sets of docking orientations generated by fast geometry-based approaches.

METHODS

Docking Sets

We used two main docking benchmarks to test our scoring function. The first set comprised the 45 unbound cases of the published ICM benchmark set.[19] Rigid-body docking poses for this ICM benchmark had been previously created by ICM-DISCO docking program.[19]

The second test set was taken from Weng's benchmark.[21] At the time when we did this work there were only 80 cases available on their web, so the cases 1ahw, 1bvk, 1dqj, and 1mlc (included in Weng's final benchmark) are missing from our benchmark. Rigid-body docking poses for Weng's benchmark set were generated by using FTDOCK (without electrostatics option)[11] or ZDOCK2.1.[12] We did not use later, upgraded versions of these programs because our focus was just to generate docking orientations based on pure geometric criteria to avoid interference of external energy terms on our scoring function.

In many cases, PDB files needed repairing to use them for calculations. For instance, incomplete side-chains were rebuilt by SCWRL 3.0,[22] a fast and efficient program for prediction of protein side-chain conformations. Residues with missing backbone atoms were removed (they were often incomplete N-terminal or C-terminal residues). Cofactors, ions and other heteroatoms were not considered.

pyDock: A New Docking Protocol

Rigid-body docking orientations were evaluated by their binding energy based on electrostatics and desolvation energy [Eq. (1)]. The pairwise electrostatics potential is based on the Coulombic electrostatics energy with a distance-dependent dielectric constant ($\varepsilon = 4.0r$) and charges from the AMBER 94 force field.[23] To avoid excessive dependence on incorrect geometries, the interatomic potential is truncated to a maximum and minimum of 1.0 and -1.0 kcal/mol, respectively. Desolvation energy is based on atomic solvation parameters (ASPs) optimized for rigid-body docking as previously described.[19] This scoring function is integrated in the pyDock docking protocol. The program pyDock is written in python and uses the MMTK set of python libraries[24] for parsing PDB files, calculating AMBER charges, and for other common tasks. The executable files of the program are available from the authors upon request.

$$E = E_{\text{ele}} + E_{\text{des}} \quad (1)$$

The potential role of van der Waals energy in the scoring of docking poses has also been evaluated. van der Waals binding energy is based on the 6–12 Lennard–Jones potential, with atomic parameters from the AMBER 94 force field. As with the electrostatics potential, to avoid too much noise from the docking of rigid-body surfaces, the van der Waals interatomic energy has been truncated to a maximum of 1.0 kcal/mol.

Success Rate: Random Success Rate

The predictive capability of pyDock was evaluated on the 80 test cases of Weng's benchmark set. Thus, the success rate was defined by the percentage of test cases in which at least one near-native docking solution (which can be acceptable or good, depending on criteria detailed below) was found within the top N solutions ($N = 10$, 20, 30, 40, 50, 100, 200, 300, 400, 500) ranked according to the new scoring function. Acceptable solutions were defined as those ones with ligand RMSD $\leq$10 Å with respect to the ligand position in the real complex structure. Good solutions were defined as those with ligand

RMSD $\leq$5 Å. For example, the success rate of pyDock to find at least one good solution within top 100 solutions would be the percentage of Weng's benchmark protein cases that have at least one good solution (RMSD $\leq$ 5 Å) within the top 100 solutions (as ranked by pyDock). The success rate of FTDOCK and ZDOCK were also evaluated in the same way as we did for pyDock, but the solutions were sorted according to their default scoring values.

In addition, we also calculated a random success rate as a reference for evaluating the docking results. The definition of a random success rate is the average chance for choosing at least one good or acceptable solution within the top N solutions (N = 10, 20, 30, 40, 50, 100, 200, 300, 400, 500) of a test protein that has X good or acceptable solutions within a total of M solutions. The probability (P) of randomly selecting at least one good or acceptable solution for each test protein was calculated according to Eq. (2), and the final random success rate was calculated as an average value of the random probabilities calculated by Eq. (2) for each test proteins:

$$\mathrm{P} = ((\mathrm{C}_1^X \times \mathrm{C}_{N-1}^{M-X}) + (\mathrm{C}_2^X \times \mathrm{C}_{N-2}^{M-X}) + \cdots + (\mathrm{C}_{N\leq X}^X \times \mathrm{C}_{N-X}^{M-X}))/\mathrm{C}_N^M \quad (2)$$

where C_k^n is the combinatorial number or binomial coefficient $\binom{n}{k} = \frac{n!}{k!(n-k)!}$, which represents the number of ways of picking k unordered outcomes from a group of n possibilities.

Optimization of the Scoring Function

We used a simplex optimization method in order to find the optimal balance between electrostatics and desolvation within the scoring function [W_{des} weighting factor in Eq. (3)]. Five random cases where FTDOCK found at least one good docking solution ($\leq$5 Å ligand RMSD) plus five other random cases where ZDOCK also found at least one good docking solution were selected as training set (1eaw, 1ewy, 1f34, 1fsk, 1i9r, 1ay7, 1bvn, 1d6r, 1kkl, 1fak). All docking solutions obtained from ZDOCK and FTDOCK for each training case were combined in a single docking set. Thus, a total of 10 docking sets with 12,000 docking orientations in each set were used to train the simplex method. The objective function was the sum, for all cases in training set, of the logarithm of the best rank (lowest rank amongst all solutions with RMSD $\leq$5 Å) after evaluation by Eq. (3). The logarithm was used here to avoid spending too much time on poorly ranked cases in the optimization procedure, and to focus instead on improving the best ranked cases. After the simplex optimization, we selected the W_{des} value that gave the minimal value for the objective function, together with the most frequently sampled W_{des} values. We evaluated the predictive capacity of all these W_{des} values in the training set. The W_{des} value that gave the best overall performance was selected.

$$E = E_{\mathrm{ele}} + W_{\mathrm{des}}\, E_{\mathrm{des}} \quad (3)$$

An external test set of 15 cases was formed by all complexes where either FTDOCK or ZDOCK obtained at least one good solution ($\leq$5 Å ligand RMSD), after excluding all complexes used for the training of the scoring function. For each test case, all docking orientations obtained from FTDOCK and ZDOCK were combined in a single docking set.

Validation of Docking Method on CAPRI Targets

The performance of the docking scoring function was evaluated in the same blind conditions as adopted for CAPRI, applying the method described here to targets 11–19.[7] Targets 11 and 12 consisted of the cohesin-dockerin complex of the cellulosome (PDB 1OHZ).[25] In both targets, the structure of unbound cohesin was used (PDB 1ANU). In Target 11, dockerin needed to be modelled: we used here the same comparative model we made with ICM for CAPRI submission, based on the NMR structure of a homologous dockerin (PDB 1DAQ), of 48% sequence identity. In Target 12, dockerin coordinates were taken from the bound conformation in the complex structure (PDB 1OHZ). Target 13 was the SAG1-antibody complex (PDB 1YNT).[26] As in the CAPRI submission, we used the coordinates of the unbound SAG1 (PDB 1KZQ), and the bound antibody (PDB 1YNT). Target 14 consisted of the protein Ser/Thr phosphatase-1 bound to MYPT1 (PDB 1S70).[27] For the phosphatase, we used here the comparative model built with ICM, based on the NMR structure of the homologous phosphatase 1-α (PDB 1FJM) of 93% sequence identity. As in CAPRI, the bound MYPT1 was used (PDB 1S70). Target 18 was xylanase and TAXI complex (PDB 1T6G).[28] We used the coordinates of unbound xylanase (PDB 1UKR), and the bound TAXI (PDB 1T6G). As in CAPRI, we added a pseudo-energy to the pyDock scoring function based on interface restraints for the xylanase residues Glu79 and Glu170, using the pyDockRST algorithm.[29] Target 19 was the ovine prion and Fab (PDB 1TPX).[30] A homology model was previously built by ICM for the ovine prion based on the structure of the homologous bovine prion (PDB 1DWY), of 95% sequence identity. The coordinates of the bound Fab were used (PDB 1TPX). Ligand RMSD was computed according to CAPRI criteria,[7] that is, RMSD of the ligand in the predicted (docking solution) versus target (X-ray structure) complexes after the receptors were optimally superimposed. Following CAPRI criteria, in the case of Target 13 only the binding domain (D1) of the ligand was considered, as the second domain moves as a rigid-body between the unbound and bound states and is not relevant for the interaction.

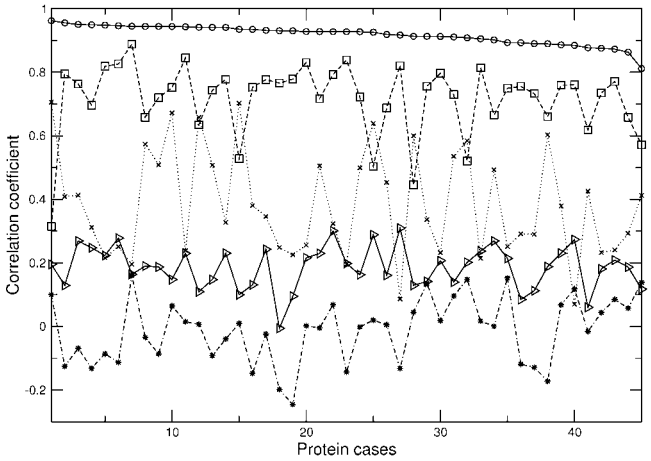

Fig. 1. Correlation between the total energy and the individual energy terms (triangles, van der Waals; crosses, electrostatics; squares, desolvation; asterisks, hydrogen-bonding) as previously reported by ICM for the rigid-body docking solutions obtained by ICM-DISCO for each one of the cases of a previous benchmark test set of 45 unbound cases.[19] Circles represent the correlation values between electrostatics + desolvation and the total energy.

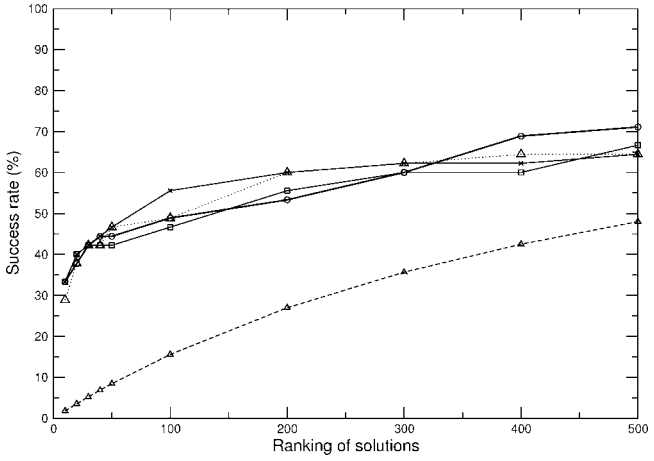

Fig. 2. Success rates (percentage of cases where at least an acceptable solution, RMSD $\leq$ 10 Å, is detected with rank smaller than the number given in abscissas) of different scoring functions on rigid-body docking sets generated by ICM for a benchmark test set of 45 unbound cases previously compiled[19]: ICM total binding energy (line with crosses); ICM electrostatics + desolvation (dotted line with triangles); ICM electrostatics + desolvation + van der Waals (line with squares); pyDock electrostatics + desolvation (line with circles). The success rates expected by random distributions of the docking poses are also shown (dashed line with diamonds).

RESULTS AND DISCUSSION

Relevance of the Different Energy Terms on Scoring Rigid-Body Docking Poses

The energy function that was previously developed to rescore ICM rigid-body docking poses[19] consisted on the following energy terms: van der Waals, electrostatics, hydrogen-bonding, and desolvation. To study the importance of each one of the individual energy terms for the scoring of the rigid-body docking solutions, we analyzed, for each docking case, the correlation between every individual energy value and the total energy. Figure 1 shows Pearson's correlation coefficient for every individual energy term of the 45 benchmark cases. We have computed also the correlation coefficient for the sum of electrostatics and desolvation, and we have sorted the cases according to these correlation values for the sake of clarity. The square of the correlation coefficient (r^2) will give us a rough percentage for the amount of variation in the total energy that is directly attributable to a specific energy term. As can be seen, electrostatics and desolvation (mostly the latter) contribute to the total scoring more than any other energy term. Desolvation is the most important term in 39 out of the 45 cases, electrostatics in 6 out of 45, while van der Waals or hydrogen-bonding is never the most important term. Moreover, the sum of electrostatics and desolvation terms alone roughly accounts for more than 70% of the total energy in all cases. The van der Waals energy term never accounted for more than 10% of the total energy. Hydrogen-bonding does not seem to contribute at all to the total scoring as its correlation coefficient values are mostly negative, and very rarely over 0.1. One would expect that hydrogen-bonding, which is known to largely contribute to conformational specificity, should be important for the discrimination between docking orientations. However, it seems that because of the rigid-body approach, the strict geometrical requirements for the formation of many of the possible intermolecular hydrogen bonds cannot be fulfilled. This clearly shows that the most relevant terms for scoring of these rigid-body docking poses were actually electrostatics and desolvation.

We have rescored the docking poses generated by ICM for the benchmark of 45 cases by using only the ICM electrostatics and desolvation energy terms. As can be seen in Figure 2, the success rates are similar to those obtained with the ICM total energy. The addition of ICM van der Waals energy to electrostatics and desolvation did not improve the predictive results (Fig. 2). Although van der Waals energy was likely to be essential during the generation of docking poses in ICM (when orientations with either excessive or poor number of intermolecular contacts needed to be filtered out), such energy term is too fine for a further evaluation of the selected docking interfaces, because of the expected number of geometrically inaccurate side-chains arisen from the rigid-body approach.

Electrostatics and Desolvation are Sufficient for Scoring of Rigid-Body Docking Poses

Having shown the importance of electrostatics and desolvation for the scoring of ICM rigid-body docking solutions, we implemented in pyDock a scoring function based only on these energy terms: electrostatics and desolvation (Methods). Desolvation in pyDock was calculated based on the same solvation parameters as those used in ICM, so the correlation between ICM and pyDock values is high. As for electrostatics, in ICM grids, minimum and maximum cutoffs were −20 and

+20, respectively. In pyDock, we found that with minimum and maximum cutoffs of −1 and 1, we could obtain a reasonable correlation of these electrostatics values with those from ICM (data not shown). The reasons for the different cutoffs can be several. On the one hand, charges in ICM are taken from ECEPP force field, whereas in pyDock are taken from AMBER. On the other hand, docking orientations obtained by ICM were minimized after each Monte Carlo step with respect to an energy function that included the electrostatics term, but they do not need to be necessarily at a minimum defined by pyDock electrostatics.

To validate the capability of the scoring procedure in pyDock to evaluate sets of rigid-body docking solutions, we used the docking sets generated by ICM-DISCO for 45 unbound cases.[19] Figure 2 shows the success rate after scoring the ICM docking solutions by Eq. (1). The success rate of pyDock, well above the one expected by random, is actually very similar to that of ICM-DISCO scoring function, which includes additional van der Waals and hydrogen bonding terms. Remarkably, an acceptable solution is found within the top 20 docking orientations in more than 40% of the cases. This clearly demonstrates that electrostatics and desolvation terms alone are sufficient for scoring of the ICM-DISCO rigid-body docking poses.

Scoring of Rigid-Body Docking Orientations Generated by FFT-Based Sampling

In the previous section we have shown that the scoring of rigid-body docking solutions with simple Coulombic electrostatics and a desolvation term that accounts for the effective water-to-interface transfer energy can be sufficient for successful prediction of near-native complex geometries. However, one can argue that ICM docking solutions were somehow optimized for this kind of electrostatics and desolvation energy function, so we need to explore to what extent our scoring function is dependent on the geometry of the docking poses. For that, we used Eq. (1) to score docking solutions generated by other docking approaches.

We ran docking simulations on the 80 docking cases from Weng's benchmark. Rigid-body docking poses were generated with the FFT-based programs FTDOCK and ZDOCK, and the resulting docking solutions were evaluated by our scoring function [Eq. (1)]. Figure 3 shows the success rate of our simple scoring function [Eq. (1)] for (A) the rigid-body docking sets generated by FTDOCK (10,000 docking solutions for each case), (B) the docking sets generated by ZDOCK (2000 per case), and (C) the combined docking sets from FTDOCK and ZDOCK (12,000 per case). The performance is slightly

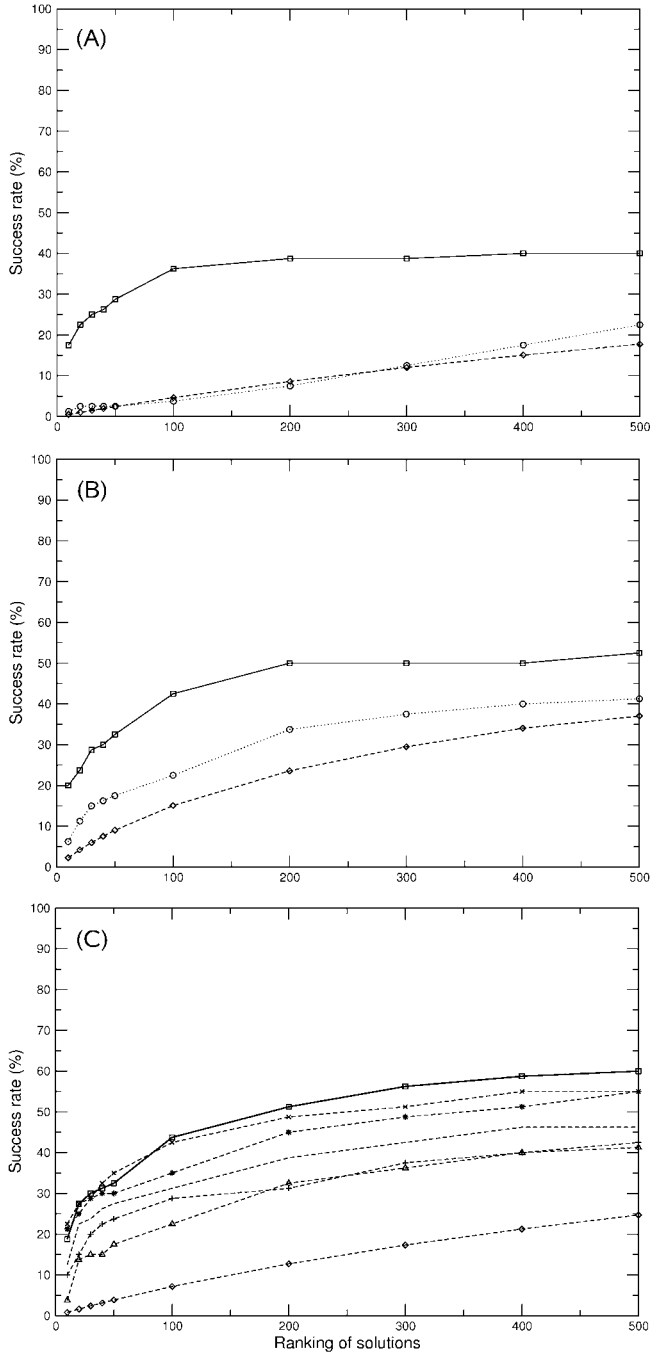

Fig. 3. Scoring by Eq. (1) of rigid-body docking sets generated for the 80 unbound cases of Weng's benchmark. Success rate is defined as the percentage of cases in which at least an acceptable docking solution (RMSD $\leq$ 10 Å) is found within the top N rigid-body docking solutions. Black line (squares) is the success rate when the docking sets are ranked by Eq. (1). Dotted line (circles) is the success rate of the default ranks obtained by the docking program used to generate the docking solutions (FTDOCK or ZDOCK). Dashed line (diamonds) is the expected success rate by random. (**A**) Rigid-body generated by FTDOCK (10,000 docking poses per case). (**B**) Rigid-body docking generated by ZDOCK (2000 docking poses per case). (**C**) Combined rigid-body docking sets from all 10,000 FTDOCK docking poses and all 2000 ZDOCK ones. For the FTDOCK and ZDOCK combined sets, van der Waals values were also added to the scoring function [Eq. (4)], and the shown success rates (dashed lines) correspond to the different weighting factors used for van der Waals: 1.0 (plus markers); 2.0 (triangles); 0.5 (no markers); 0.2 (stars); 0.1 (crosses).

better for the ZDOCK docking set than for the FTDOCK one. This could be just a statistical effect as the total number of ZDOCK docking solutions is smaller. To check this, we selected only the first 2000 docking solutions in FTDOCK, but the results did not improve (data not shown). Interestingly, when we took the combined sets from FTDOCK and ZDOCK, the success rate further increased over the results on the separate sets. We can rationalize this by the fact that there are more cases with at least a near-native solution, which is efficiently detected by our scoring function. The success rate of our electrostatics + desolvation scoring function is higher than the default score given by FTDOCK or ZDOCK, and it is well above the expected random success rate. This indicates that the appropriate combination of a simple description of electrostatics and desolvation function can be sufficient for efficient ranking of the near-native geometries among a large number of rigid-body docking candidates. Table I shows the best pyDock rank for any acceptable ($\leq$10 Å) or good ($\leq$5 Å) solution, in the combined docking sets obtained from FTDOCK and ZDOCK for every docking case of the benchmark. As expected, the predictive results are better for the "rigid-body" cases, slightly worse for the "medium difficulty" cases, and much worse for the "difficult" ones. In our previous work,[29] our scoring function applied to FTDOCK-based docking poses found acceptable solutions within the lowest-scoring 50 docking solutions in just 1 out of 10 cases, a success rate clearly poorer than the one found here for the overall benchmark. However, that previous test set, much smaller than that of the present work, was formed only by cases that necessarily had sufficient number of homologous sequences, as the point was not to test the scoring function itself, but the use of distance restraints derived from evolutionary information as a filtering step in docking.[29] Most of those cases would fall under the categories of "medium" or "difficult" complexes in our current benchmark, in which the success rate for the top 50 solutions is actually of around 10% (Table I).

We saw in the previous section that van der Waals term was not relevant for scoring of ICM docking poses, but as it has been previously discussed, this might be closely related to the specific method used for the generation of the docking poses. Therefore we have evaluated whether docking poses generated by FTDOCK or ZDOCK might need this energy term (for instance, to detect interfaces with possible excessive or poor number of intermolecular contacts). As can be seen in Figure 3(C), when we added the van der Waals term to the pyDock scoring function [Eq. (4)], the results varied depending on the weighting factor (W_{vdw}) used for this term. Large weighting factor values ($W_{\mathrm{vdw}} = 0.5, 1.0, 2.0$) got clearly worse results. Better results were obtained with smaller weighting factors, but in the best of the cases ($W_{\mathrm{vdw}} = 0.1$), the success rates were very similar to those obtained by electrostatics and desolvation alone. Giving the additional computational cost of introducing a new term in the scoring function, inclusion of van der Waals was clearly not justified, and therefore we used Eq. (1) as pyDock scoring function.

$$E = E_{\mathrm{ele}} + E_{\mathrm{des}} + W_{\mathrm{vdw}}\, E_{\mathrm{vdw}} \quad (4)$$

This overall performance of the electrostatics plus desolvation scoring function on the FTDOCK and ZDOCK-generated docking sets gives an estimation of the expected success rate in a real docking scenario. Therefore, when we use Eq. (1) to score combined docking sets obtained from FTDOCK and ZDOCK, we can expect at least a near-native solution within the 100 top solutions in around half of the cases. This global success rate is quite high, but it is not yet optimal. One possible explanation could be related to the actual limitations of the scoring function to detect the near-native solutions in certain cases. However, another reason is that FTDOCK and ZDOCK do not always generate an acceptable solution (i.e. $\leq$10 Å) among the docking candidates. In the present docking benchmark, FTDOCK creates at least an acceptable solution in 52 out of the 80 cases, and ZDOCK in 58 out of the 80 cases. When FTDOCK and ZDOCK docking sets are combined, an acceptable solution is found in 63 out of the 80 cases. This limitation is not related with our scoring function, and may make it difficult to evaluate its real predictive capabilities. Thus, to explore the real efficiency of our scoring function, it should be tested on docking sets that contain near-native solutions. For that, we did a series of tests. First, we manually added the optimal solution to every docking set, formed by superimposing unbound receptor and ligand onto the complex coordinates. As expected, when all the docking sets had at least one acceptable solution (including these manually added optimal solutions), the success rate of our scoring function improved (Fig. 4). The second test was selecting only those docking sets that contain at least an acceptable solution (RMSD $\leq$ 10 Å). The results are shown in Figure 5, and they are very similar to the ones obtained for the docking sets with the manually-added optimal solution. Finally, we tested our scoring function on those cases where at least one good solution (RMSD $\leq$ 5 Å) is found (14 out of 80 cases in FTDOCK; 23 out of 80 cases in ZDOCK; 30 out of 80 cases in the combined FTDOCK + ZDOCK docking sets). As can be seen in Figure 6, the success rates are higher than when considering all docking sets, and similar to the ones obtained with docking sets with at least one acceptable solution. This clearly shows that, when the docking method is able to generate good docking orientations, these are very well ranked by our scoring function. Thus, if FTDOCK generates at least a good solution for a given case, our scoring function will rank it within the 100 lowest-energy solutions with more than 40% probability. As for ZDOCK, provided it is able to generate at least a good solution, our scoring function will rank it within the 100 lowest-energy solutions with more than 55% probability. To disregard statistical effects (given that we have 10,000 docking orientations in FTDOCK vs. 2000 in ZDOCK), we have also selected only those

TABLE I. pyDock Results on Weng's Docking Benchmark

Receptor description/ligand description	Complex	Receptor	Ligand	Acceptable solution[a]		Good solution[b]	
				RANK	RMSD	RANK	RMSD
Rigid-body (59)							
Porcine trypsin/soybean trypsin inhibitor	1AVX_A:B	1QQU_A	1BA7_B	60	8.9	–	–
Barnase/barstar	1AY7_A:B	1RGH_B	1A19_B	221	9.1	239	3.1
Alpha-amylase/tendamistat	1BVN_P:T	1PIG_	1HOE_	2	4.3	2	4.3
Bovine chymotrypsinogen/PSTI	1CGI_E:I	2CGA_B	1HPT_	8	5.6	926	3.0
Bovine trypsin/Bowman-Birk inhibitor	1D6R_A:I	2TGT_	1K9B_A	232	8.4	6232	3.3
Ribonuclease A/Rnase inhibitor	1DFJ_E:I	9RSA_B	2BNH_	1	3.9	1	3.9
Adrenoxin reductase/adrenoxin	1E6E_A:B	1E1N_A	1CJE_D	37	8.8	–	–
Matriptase/BPTI	1EAW_A:B	1EAX_A	9PTI_	182	5.9	419	4.2
Ferredoxin reductase/ferredoxin	1EWY_A:C	1GJR_A	1CZP_A	57	9.4	386	4.2
D102N Trypsin/ecotin	1EZU_C:AB	1TRM_A	1ECZ_AB	407	5.9	–	–
Porcine pepsin/ascaris inhibitor 3	1F34_A:B	4PEP_	1F32_A	29	6.9	56	4.2
Kallikrein/hirustatin	1HIA_AB:I	2PKA_XY	1BX8_	58	8.7	–	–
Acetylcholinesterase/fasciculin	1MAH_A:F	1J06_B	1FSC_	7	8.8	12	4.6
Bovine trypsin/CMTI-1 squash inhibitor	1PPE_E:I	1BTP_	1LU0_A	1	3.3	1	3.3
alpha-amylase/RAGI inhibitor	1TMQ_A:B	1JAE_	1B1U_A	18	10.0	69	4.4
Uracyl-DNA glycosylase/glycosylase inhibitor	1UDI_E:I	1UDH_	2UGI_B	1	3.3	1	3.3
Methylamine dehydrogenase/amicyanin	2MTA_HL:A	2BBK_JM	2RAC_A	183	9.8	–	–
Cyt C peroxidase/cytochrome C	2PCC_A:B	1CCP_	1YCC_	8	9.2	–	–
Subtilisin/streptomyces subtilisin inhibitor	2SIC_E:I	1SUP_	3SSI_	7	9.0	259	5.0
Subtilisin/chymotrypsin inhibitor 2	2SNI_E:I	1UBN_A	2CI2_I	15	2.0	15	2.0
Colicin E7 nuclease/Im7 immunity protein	7CEI_A:B	1UNK_D	1M08_B	2	9.8	26	4.7
Fab/ HIV-1 capsid protein p24	1E6J_HL:P	1E6O_HL	1A43_	6	7.9	9	4.5
Fab D3H44/tissue factor	1JPS_HL:T	1JPT_HL	1TFH_B	4864	10.0	–	–
Fv D1.3/HEW lysozyme	1VFB_AB:C	1VFA_AB	8LYZ_	1	8.1	317	4.2
Fab E8/cytochrome C	1WEJ_HL:F	1QBL_HL	1HRC_	758	7.1	–	–
Fab/Flu virus hemagglutinin	2VIS_AB:C	1GIG_LH	2VIU_ACE	–	–	–	–
Ran GTPase/nuclear transport factor 2	1A2K_C:AB	1QG4_A	1OUN_AB	–	–	–	–
Cyclophilin/HIV capsid	1AK4_A:D	2CPL_	1E6J_P	–	–	–	–
MHC Class 1 HLA-A2/T-cell CD8 coreceptor	1AKJ_AB:DE	2CLR_DE	1CD8_AB	935	9.3	3986	3.4
FKBP binding protein/TGFbeta receptor	1B6C_A:B	1D6O_A	1IAS_A	7	8.8	–	–
CDK2 kinase/Ckshs1	1BUH_A:B	1HCL_	1DKS_A	142	6.7	–	–
Rac GTApase/p67 Phox	1E96_A:B	1MH1_	1HH8_A	16	6.6	–	–
Sporulation response factor B/sporulation response factor F	1F51_AB:E	1IXM_AB	1SRR_C	20	9.5	384	4.4
Staphylococcus protein A/human Fc fragment	1FC2_C:D	1BDD_	1FC1_AB	–	–	–	–
Gt-alpha/RGS9	1FQJ_A:B	1TND_C	1FQI_A	1746	10.0	–	–
GRB2 C-ter SH3 domain/GRB2 N-ter SH3 domain	1GCQ_B:C	1GRI_B	1GCP_B	1820	8.8	–	–
Epstein–Barr virus receptor CR2/complement C3	1GHQ_A:B	1C3D_	1LY2_A	2031	6.9	–	–
Rac GTPase/*Pseudomonas* toxin GAP dom.	1HE1_C:A	1MH1_	1HE9_A	156	7.9	5878	3.9
Rac GTPase/arfaptin	1I4D_D:AB	1MH1_	1I49_AB	99	7.0	–	–
Adenovirus fiber knob protein/adenovirus receptor	1KAC_A:B	1NOB_F	1F5W_B	1470	10.0	–	–
MHC class 2 HLA-DR1/*Staphylococcus* enterotoxin C3	1KLU_AB:D	1H15_AB	1STE_	–	–	–	–
TGF-beta/TGF-beta receptor	1KTZ_A:B	1TGK_	1M9Z_A	1077	8.7	–	–
Actin/vitamin D binding protein	1KXP_A:D	1IJJ_B	1KW2_B	2	9.4	–	–

TABLE I. (Continued)

Receptor description/ligand description	Complex	Receptor	Ligand	Acceptable solution[a]		Good solution[b]	
				RANK	RMSD	RANK	RMSD
Viral chemokine binding p. M3/chemokine Mcp1	1ML0_AB:D	1MKF_AB	1DOL_	17	8.8	48	5.0
CD2/CD58	1QA9_A:B	1HNF_	1CCZ_A	361	8.9	–	–
Transthyretin/retinol binding protein	1RLB_ABCD:E	2PAB_ABCD	1HBP_	5278	8.9	–	–
T-cell receptor beta/*Staphylococcus* enterotoxin B	1SBB_A:B	1BEC_	1SE4_	–	–	–	–
Actin/profilin	2BTF_A:P	1IJJ_B	1PNE_	143	8.0	–	–
Fab/vEGF	1BJ1_HL:VW	1BJ1_HL	2VPF_GH	70	9.2	80	4.1
Fab/Birch pollen antigen Bet V1	1FSK_BC:A	1FSK_BC	1BV1_	1	7.5	8	4.8
Fab/Cd40 ligand	1I9R_HL:ABC	1I9R_HL	1ALY_ABC	98	2.9	98	2.9
Fab/Factor VIII domain C2	1IQD_AB:C	1IQD_AB	1D7P_M	13	9.4	–	–
Fab/potassium Channel Kcsa	1K4C_AB:C	1K4C_AB	1JVM_ABCD	2829	9.8	–	–
camel VHH/pancreatic alpha-amylase	1KXQ_H:A	1KXQ_H	1PPI_	11	6.7	28	2.6
Fab/Flu virus neuraminidase N9	1NCA_HL:N	1NCA_HL	7NN9_	43	5.0	43	5.0
Fab N10/Staphylococcal nuclease	1NSN_HL:S	1NSN_HL	1KDC_	650	4.0	650	4.0
Fv/human chorionic gonadotropin	1QFW_HL:AB	1QFW_HL	1HRP_AB	7	6.1	–	–
Fv/human chorionic gonadotropin	1QFW_IM:AB	1QFW_IM	1HRP_AB	233	3.9	233	3.9
Fab Jel42/HPr	2JEL_HL:P	2JEL_HL	1POH_	53	7.3	–	–
Medium difficulty (13)							
Chymotrypsin/Eglin C	1ACB_E:I	2CGA_B	1EGL_	63	8.9	4499	5.0
HPr kinase C-ter domain/HPr	1KKL_ABC:H	1JB1_ABC	2HPR_	372	9.7	–	–
Fab/Taq polymerase	1BGX_HL:T	1AY1_HL	1CMW_A	–	–	–	–
Gi-alpha/Gi-beta,gamma	1GP2_A:BG	1GIA_	1TBG_DH	10	9.6	–	–
CDC42 GTPase/CDC42 GAP	1GRN_A:B	1A4R_A	1RGP_	27	9.4	3962	4.3
Ras GTPase/PIP3 kinase	1HE8_B:A	821P_	1E8Z_A	253	7.6	–	–
Ran GTPase/RCC1	1I2M_A:B	1QG4_A	1A12_A	1501	8.7	–	–
14–3–3 protein/serotonin N–acteylase	1IB1_AB:E	1QJB_AB	1KUY_A	5193	9.1	–	–
Botrocetin/Von Willebrand Factor dom. A1	1IJK_BC:A	1FVU_AB	1AUQ_	1661	9.7	–	–
Ran GTPase/Ran GAP	1K5D_AB:C	1RRP_AB	1YRG_B	–	–	–	–
Von Willebrand Factor dom. A1/Glycoprotein IB-alpha	1M10_A:B	1AUQ_	1M0Z_B	–	–	–	–
Nitrogenase Mo-Fe protein/Nitrogenase Fe protein	1N2C_ABCD:EF	3MIN_ABCD	2NIP_AB	–	–	–	–
Ras GTPase/Ras GAP	1WQ1_R:G	6Q21_D	1WER_	192	8.1	–	–
Difficult (8)							
Actin/Dnase I	1ATN_A:D	1IJJ_B	3DNI_	–	–	–	–
beta2-microglobulin/transferrin receptor ectodom	1DE4_AB:CF	1A6Z_AB	1CX8_AB	–	–	–	–
Erythropoietin/EPO receptor	1EER_A:BC	1BUY_A	1ERN_AB	–	–	–	–
Coagulation factor VIIa/Soluble tissue factor	1FAK_HL:T	1QFK_HL	1TFH_B	9355	9.4	–	–
CDK inhibitor 3/CDK2 kinase	1FQ1_A:B	1FPZ_F	1B39_A	–	–	–	–
Actin/gelsolin	1H1V_A:G	1IJJ_B	1D0N_B	–	–	–	–
Ran GTPase/importin beta	1IBR_A:B	1QG4_A	1F59_A	–	–	–	–
Fab 28/HIV1 reverse transcriptase	2HMI_CD:AB	2HMI_CD	1S6P_AB	–	–	–	–

[a]Best rank of any acceptable solution (≤10 Å) found by pyDock within the combined set of docking poses generated by FTDOCK and ZDOCK. Ligand RMSD for this solution is shown. When there is no acceptable solution generated by either FTDOCK or ZDOCK, it is indicated as "–". All these acceptable solutions are classified as "acceptable" (or better) according to CAPRI criteria.
[b]Best rank of any good solution (≤5 Å) found by pyDock. Ligand RMSD for this solution is shown. All these good solutions are classified as "medium" or "high" according to CAPRI criteria.

cases where FTDOCK finds at least a good solution within the first 2000 solutions (12 out of 80 cases) and have used only the first 2000 solutions for the analysis, but the results do not significantly change (data not shown). This suggests that the rigid-body solutions generated by ZDOCK are perhaps geometrically more appropriate for our scoring function than those of FTDOCK (of course, given the program versions and the conditions of this work). In any case, these results show that our scoring function discriminates quite efficiently the near-native solutions when they are within the docking set.

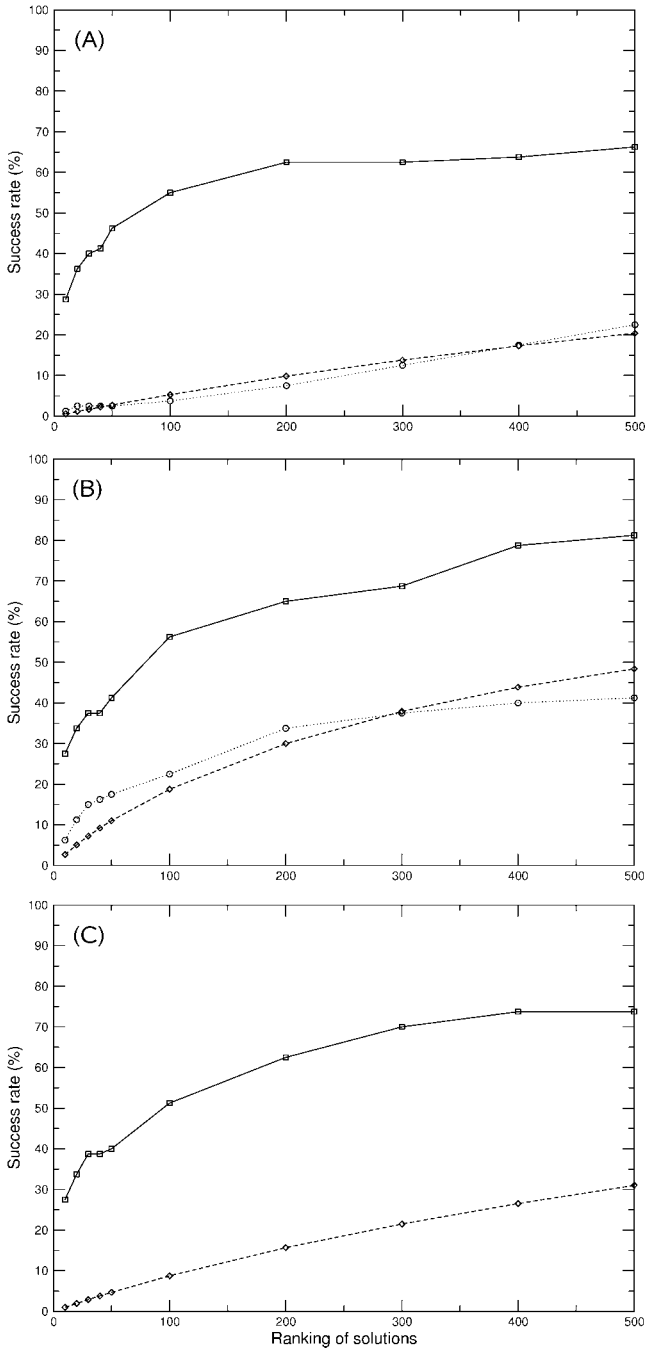

Fig. 4. Same rigid-body docking sets as in Figure 3, but after manually adding the optimal solution generated by superimposing unbound receptor and ligand molecules onto the crystal structure of the complex. Success rates are defined as in Figure 3. Black line (square) is the success rate when the docking sets are ranked by Eq. (1). Dotted line (circle) is the success rate of the default ranks obtained by the docking program used to generate the docking solutions (FTDOCK or ZDOCK). Dashed line (diamonds) is the expected success rate by random. (**A**) Rigid-body generated by FTDOCK (10,000 docking poses per case). (**B**) Rigid-body docking generated by ZDOCK (2000 docking poses per case). (**C**) Combined rigid-body docking sets from all 10,000 FTDOCK docking poses and all 2000 ZDOCK ones.

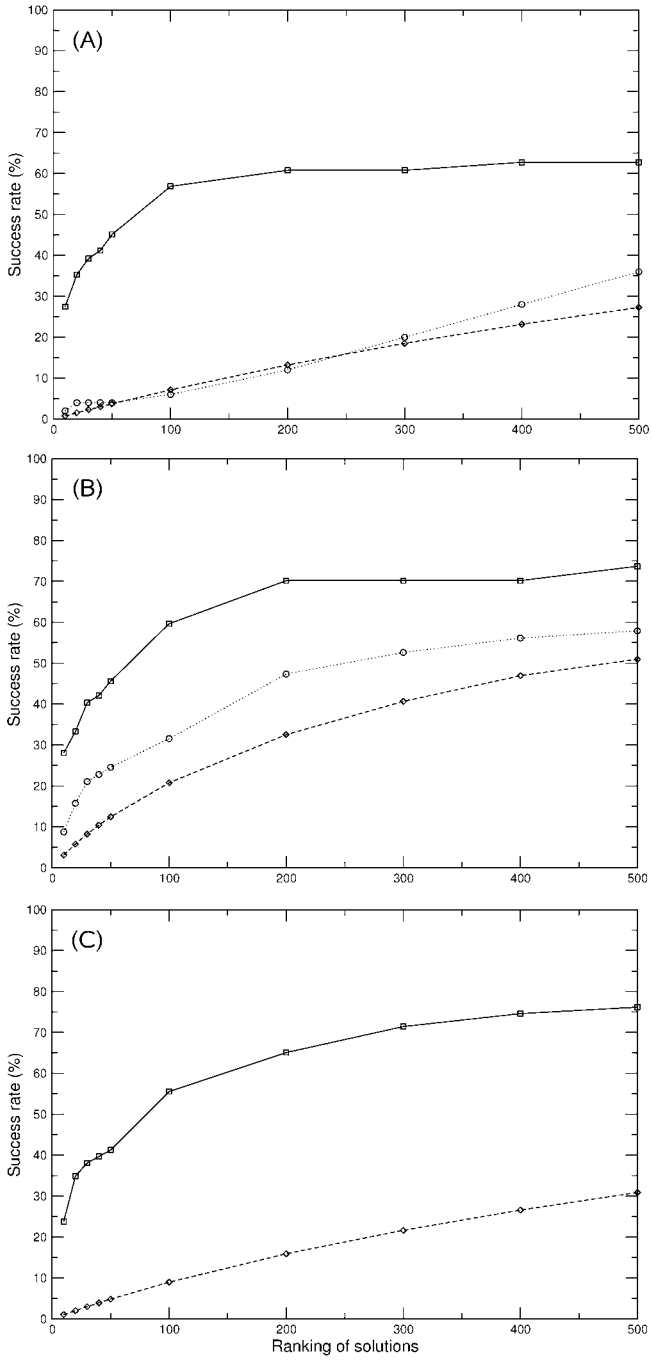

Fig. 5. Scoring by Eq. (1) of rigid-body docking sets that contains at least an acceptable docking solution (RMSD $\leq$ 10 Å). Success rates are defined as in Figure 3. Black line (squares) is the success rate when the docking sets are ranked by Eq. (1). Dotted line (circles) is the success rate of the default ranks obtained by the docking program used to generate the docking solutions (FTDOCK or ZDOCK). Dashed line (diamonds) is the expected success rate by random. (**A**) Rigid-body generated by FTDOCK (10,000 docking poses per case). (**B**) Rigid-body docking generated by ZDOCK (2000 docking poses per case). (**C**) Combined rigid-body docking sets from all 10,000 FTDOCK docking poses and all 2000 ZDOCK ones.

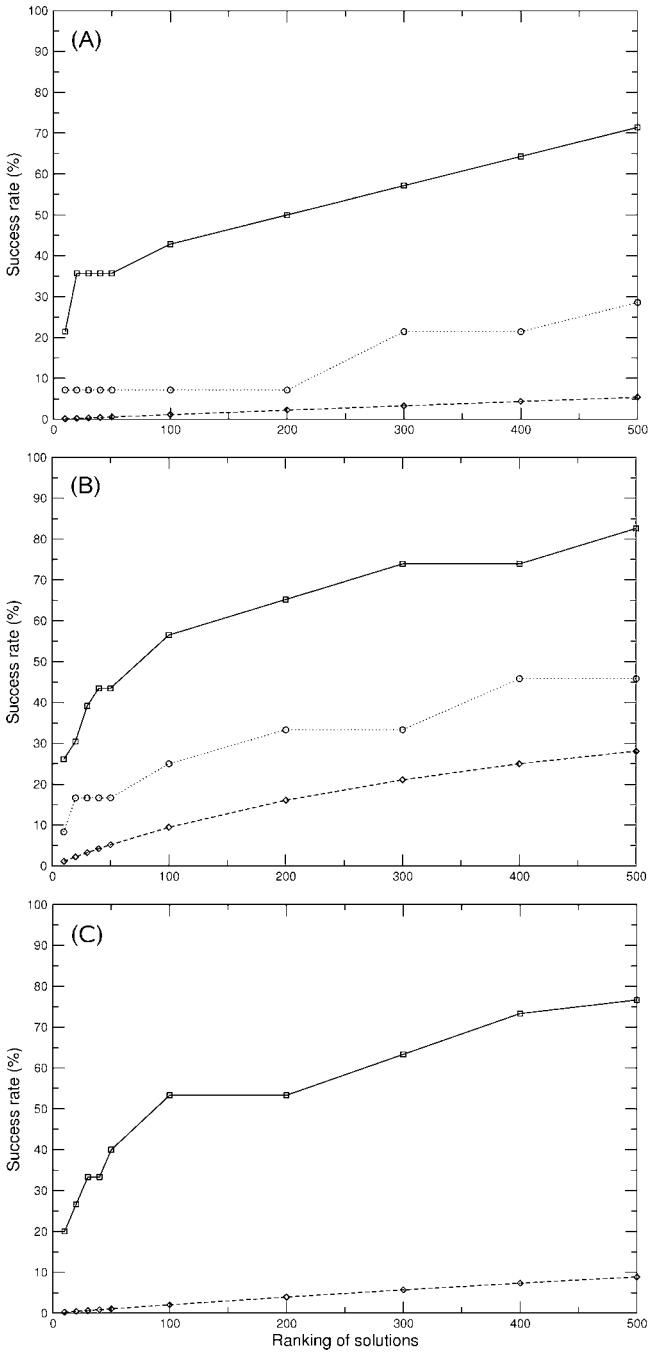

Fig. 6. Scoring by Eq. (1) of rigid-body docking sets that contains at least a good docking solution (RMSD $\leq$ 5 Å). Success rates refer to good docking solutions (RMSD $\leq$ 5 Å). Black line (squares) is the success rate when the docking sets are ranked by Eq. (1). Dotted line (circles) is the success rate of the default ranks obtained by the docking program used to generate the docking solutions (FTDOCK or ZDOCK). Dashed line (diamonds) is the expected success rate by random. (**A**) Rigid-body generated by FTDOCK (10,000 docking poses per case). (**B**) Rigid-body docking generated by ZDOCK (2000 docking poses per case). (**C**) Combined rigid-body docking sets from all 10,000 FTDOCK docking poses and all 2000 ZDOCK ones.

The success rates reported by the authors of FTDOCK and ZDOCK are slightly different from those we found when we ran the programs. For instance, in the ZDOCK2.1 paper, they found hits within the top 1000 solutions in 80% of the cases, whereas in our case, we found hits within the top 2000 solutions in 58 out of 80 cases. The small difference could be due to several factors. First, it could be due to the existence of additional filtering steps. For instance, in the case of FTDOCK, they clearly indicate that they used biological filtering (e.g. residues known to be at the interface, mutational data, sequence conservation, etc.); and in the case of ZDOCK, at least the antibody–antigen complexes have been constrained to the CDR areas in the antibody, whereas here we have applied automatically our scoring function with no other restraint. Another factor could be the different criteria used to define a hit. For instance, in ZDOCK they consider a hit if a docking pose has <2.5 Å RMSD for all interface C^{α} atoms. However, we have found in the CAPRI results that there could be docking poses with <2.5 Å of interface RMSD while having >20 Å of ligand RMSD. These docking poses would not be considered a hit according to our criteria (ligand RMSD $\leq$ 10 Å). For the sake of simplicity, we have decided to use here the ligand RMSD as a single evaluating measure, although it is true that in a few cases, the quality of some solutions could be further "improved" by using additional measures such as interface RMSD or fraction of native contacts (as in CAPRI). In any case, we have checked that all solutions classified here as "acceptable" would be at least of "acceptable" or better quality under CAPRI criteria, and that all solutions defined here as "good" would be "medium" or "high" according to CAPRI criteria. Thus, the success rates shown throughout this work (based on ligand RMSD alone) would be virtually the same, if not higher, when calculated according to CAPRI criteria.

In Search of a Better Balance of Electrostatics and Desolvation

The performance of our scoring function consisting on electrostatics plus desolvation has been shown to be quite satisfactory. However, in previously described docking results, similar energy terms were used in addition to van der Waals and hydrogen-bonding potentials,[19] so we wondered whether the balance between electrostatics and desolvation could be further improved perhaps to compensate the absence of other possible energy terms. Therefore, we tried to optimize the initial 1:1 balance between electrostatics and desolvation, modifying the factor of the desolvation term (W_{des}), while keeping fixed the electrostatics term.

Using the optimization procedure described in Methods, we found an optimal value $W_{\mathrm{des}} = 0.4$. The optimization procedure was repeated with different training sets, and the obtained value was the same. We cross-validated the optimized scoring function [Eq. (3), with $W_{\mathrm{des}} = 0.4$) on an external test set formed by cases where either FTDOCK or ZDOCK found at least one good solution, and which were not used during the training stage. The combined docking sets used here were

TABLE II. pyDock Results on CAPRI Targets

Target number	Receptor/ligand	Rank	Ligand RMSD[a]	Interface RMSD[b]	f(nat)[c]	Quality[d]	Additional Criteria[e]
11	Cohesin/dockerin (unbound/homology model)	10	11.7	5.6	0.333	*	
12	Cohesin/dockerin (unbound/bound)	10	9.1	5.0	0.222	*	
13	SAG1/antibody (unbound / bound)	3	1.8	1.1	0.919	**	
14	Protein phosphatase 1- β/MIPT1 (homology model/bound)	7	22.0	14.9	0.000	–	
18	Xylanase/TAXI (unbound/bound)	4	4.4	1.8	0.941	**	Restraint added for interface residues Glu79 and Glu170 during docking
19	Prion/FAB (homology model/bound)	10	2.0	0.9	0.846	***	

[a]RMSD of the ligand C^{α} atoms with respect to the real complex structure after superimposing only receptor atoms.
[b]RMSD of the receptor and ligand interface backbone atoms with respect to the real structure, when all receptor and ligand interface backbone atoms are superimposed.
[c]Fraction of native contacts, that is, fraction of total residue contacts that are also found in the real complex structure (a contact is defined by a pair of residues, from receptor and ligand respectively, that have at least one atom at less than 5 Å of distance from the other residue).
[d]Quality of the predicted result is judged by comparison with the real structure, applying evaluation criteria analogue to those of CAPRI (***, good prediction; **, medium; *, acceptable).
[e]Additional criteria used to filter docking solutions, as previously done in CAPRI.

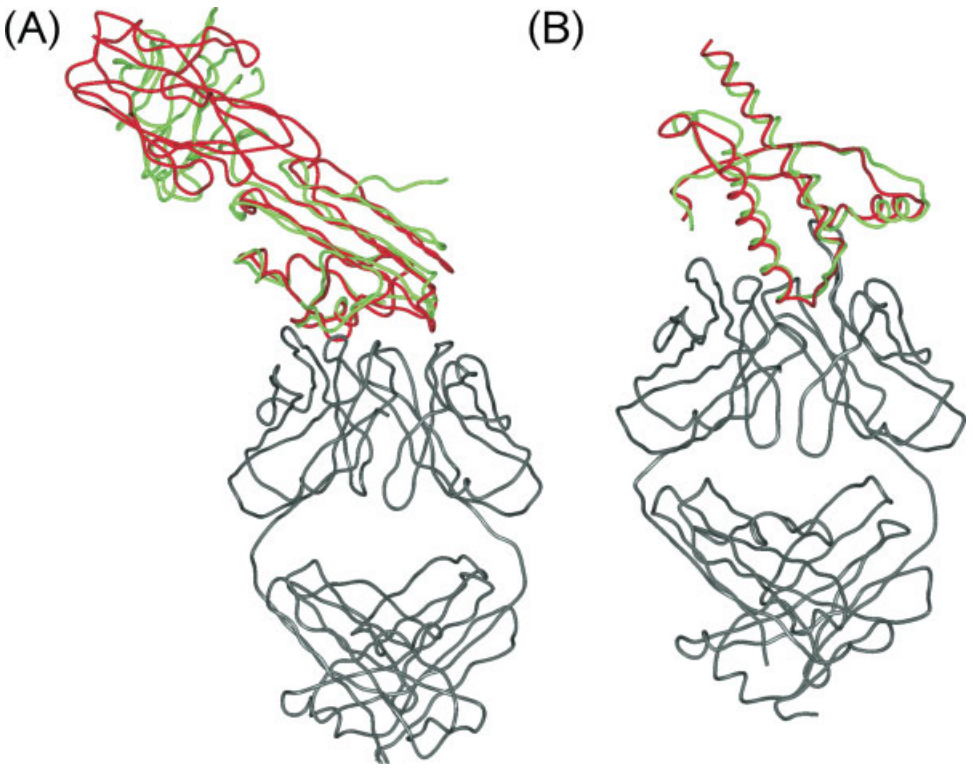

Fig. 7. Good-accuracy docking models obtained by pyDock for CAPRI targets (receptor in gray; ligand in red). (**A**) Target 13; (**B**) Target 19. Crystallographic structure of the complex is shown in green, after superimposing the receptor molecule onto that of the model.

formed by solutions generated by FTDOCK and by ZDOCK. A good solution was found within the top 100 solutions in more than 50% of the cases. To see if the scoring function was dependent on the docking method, we evaluated the predictive performance on FTDOCK and ZDOCK docking sets by separate. The performance on the separate test sets was slightly different, with better results on the ZDOCK docking sets. In both cases, the resulting ranking from the optimal function were only slightly better than the original ranking before optimization (except for the solutions ranked 200–500, where ZDOCK original scoring worked slightly better).

As a further test, we tried to optimize the W_{des} factor separately for FTDOCK and ZDOCK docking sets, obtaining very similar values. This confirmed that the obtained W_{des} was the best possible obtained. However, the performance of the optimized scoring function on the external test sets was not significantly better than the performance of the original scoring function [Eq. (1)], even if we consider all docking cases, including those on the training sets (data not shown). Given that the optimization procedure seemed to have technically worked well, this suggests that the balance between electrostatics and desolvation in the original function was already very close to optimal.

Validation of pyDock on CAPRI Targets

We tested how our docking protocol pyDock would have performed in the CAPRI experiments. For that, we applied our docking protocol to the CAPRI targets 11–19,[7] in which the new optimized desolvation was used.[20] We tried to reproduce exactly the same blind conditions as the group in which one of us participated (Fernandez-Recio, Totrov, and Abagyan)[20] had while using ICM in the CAPRI experiment. In those cases where a model needed to be built, we used the models we previously created with ICM. However, in Target 13, in difference with ICM in CAPRI,[20] we did not need to filter docking solutions by CDR contacts, and therefore we sorted the solutions just by binding energy. Actually, even better results than the ones shown here would have been obtained by filtering docking solutions with the same criteria as in CAPRI (data not shown). In Target 18 we used the same restraints as in CAPRI. The results are shown in Table II. Five out of the six targets would have been predicted with at least acceptable accuracy (as compared with six that were predicted with ICM). For two of the cases (targets 13 and 19), the models obtained had excellent accuracy (ligand RMSD of 1.8 and 2.0 Å, respectively) as can be seen in Figure 7. Moreover, their quality was actually better than that of the models generated by ICM for these CAPRI targets (ligand RMSD of 11.1 and 4.1 Å, respectively).[20] Target 13 has been given two stars (Table II) because of interface RMSD >1.0, but both the ligand RMSD and fraction of native contacts indicates that the model is very close to the X-ray solution. In the only failing case (Target 14), a solution ranked 19 was found with RMSD 1.3 Å. Although this obviously would have not been admitted as a submission in a real CAPRI test (since only 10 models are allowed), it is quite positive result. In summary, this validates the excellent performance of our simple approach for scoring of rigid-body docking poses.

CONCLUSIONS

We have shown that, given a large set of rigid-body docking poses that contains at least one near-native conformation, our scoring function can place it within the top 100 solutions in more than half of the cases (56%), and within the top 20 solutions in more than a third of the cases (37%). This presents an advantage for further refinement algorithms that can only be applied to a few rigid-body docking solutions. The revaluated docking sets could also be used for prediction of the interaction sites. The performance of pyDock is similar, if not superior, to that of the most competitive scoring functions used in rigid-body docking approaches, even though some of the other functions use additional energy terms to score the docking orientations. This suggests that both electrostatics and desolvation energy, especially the latter, are the two essential factors that drive rigid-body protein–protein association.

ACKNOWLEDGMENTS

The authors are grateful to Michael Sternberg for the use of FTDOCK, and to Zhiping Weng for the use of ZDOCK2.1 and the docking benchmark. T.M.-K.C. was recipient of a Cambridge Overseas Trust Fellowship. We are grateful to Molsoft for the use of ICM-Browser.

REFERENCES

1. Sali A, Glaeser R, Earnest T, Baumeister W. From words to literature in structural proteomics. Nature 2003;422:216–225.
2. Russell RB, Alber F, Aloy P, Davis FP, Korkin D, Pichaud M, Topf M, Sali A. A structural perspective on protein–protein interactions. Curr Opin Struct Biol 2004;14:313–324.
3. Smith GR, Sternberg MJ. Prediction of protein–protein interactions by docking methods. Curr Opin Struct Biol 2002;12:28–35.
4. Gray JJ. High-resolution protein–protein docking. Curr Opin Struct Biol 2006;16:183–193.
5. Bonvin AM. Flexible protein–protein docking. Curr Opin Struct Biol 2006;16:194–200.
6. Mendez R, Leplae R, De Maria L, Wodak SJ. Assessment of blind predictions of protein–protein interactions: current status of docking methods. Proteins 2003;52:51–67.
7. Mendez R, Leplae R, Lensink MF, Wodak SJ. Assessment of CAPRI predictions in rounds 3–5 shows progress in docking procedures. Proteins 2005;60:150–169.
8. Vakser IA, Aflalo C. Hydrophobic docking: a proposed enhancement to molecular recognition techniques. Proteins 1994;20:320–329.
9. Ten Eyck LF, Mandell J, Roberts VA, Pique ME. Surveying molecular interactions with DOT. New York: ACM Press; 1995. p 22.
10. Katchalski-Katzir E, Shariv I, Eisenstein M, Friesem AA, Aflalo C, Vakser IA. Molecular surface recognition: determination of geometric fit between proteins and their ligands by correlation techniques. Proc Natl Acad Sci USA 1992;89:2195–2199.
11. Gabb HA, Jackson RM, Sternberg MJ. Modelling protein docking using shape complementarity, electrostatics and biochemical information. J Mol Biol 1997;272:106–120.
12. Chen R, Weng Z. A novel shape complementarity scoring function for protein–protein docking. Proteins 2003;51:397–408.
13. Palma PN, Krippahl L, Wampler JE, Moura JJ. BiGGER: a new (soft) docking algorithm for predicting protein interactions. Proteins 2000;39:372–384.
14. Ritchie DW, Kemp GJ. Protein docking using spherical polar Fourier correlations. Proteins 2000;39:178–194.
15. Gray JJ, Moughon S, Wang C, Schueler-Furman O, Kuhlman B, Rohl CA, Baker D. Protein–protein docking with simultaneous optimization of rigid-body displacement and side-chain conformations. J Mol Biol 2003;331:281–299.
16. Fernandez-Recio J, Totrov M, Abagyan R. Soft protein–protein docking in internal coordinates. Protein Sci 2002;11:280–291.
17. Dominguez C, Boelens R, Bonvin AM. HADDOCK: a protein–protein docking approach based on biochemical or biophysical information. J Am Chem Soc 2003;125:1731–1737.
18. Fernandez-Recio J, Totrov M, Abagyan R. ICM-DISCO docking by global energy optimization with fully flexible side-chains. Proteins 2003;52:113–117.

19. Fernandez-Recio J, Totrov M, Abagyan R. Identification of protein–protein interaction sites from docking energy landscapes. J Mol Biol 2004;335:843–865.
20. Fernandez-Recio J, Abagyan R, Totrov M. Improving CAPRI predictions: optimized desolvation for rigid-body docking. Proteins 2005;60:308–313.
21. Mintseris J, Wiehe K, Pierce B, Anderson R, Chen R, Janin J, Weng Z. Protein–protein docking benchmark 2.0: an update. Proteins 2005;60:214–216.
22. Canutescu AA, Shelenkov AA, Dunbrack RLJ. A graph-theory algorithm for rapid protein side-chain prediction. Protein Sci 2003;12:2001–2014.
23. Cornell WD, Cieplak P, Bayly CI, Gould IR, Merz KM, Ferguson DM, Spellmayer DC, Fox T, Caldwell JW, Kollman PA. A second generation force field for the simulation of proteins, nucleic acids, and organic molecules. J Am Chem Soc 1995;117:5179–5197.
24. Hinsen K. The molecular modelling toolkit: a new approach to molecular simulations. J Comput Chem 2000;21:79–85.
25. Carvalho AL, Dias FM, Prates JA, Nagy T, Gilbert HJ, Davies GJ, Ferreira LM, Romao MJ, Fontes CM. Cellulosome assembly revealed by the crystal structure of the cohesin-dockerin complex. Proc Natl Acad Sci USA 2003;100:13809–13814.
26. Graille M, Stura EA, Bossus M, Muller BH, Letourneur O, Battail-Poirot N, Sibai G, Gauthier M, Rolland D, Le Du MH, Ducancel F. Crystal structure of the complex between the monomeric form of Toxoplasma gondii surface antigen 1 (SAG1) and a monoclonal antibody that mimics the human immune response. J Mol Biol 2005;354:447–458.
27. Terrak M, Kerff F, Langsetmo K, Tao T, Dominguez R. Structural basis of protein phosphatase 1 regulation. Nature 2004; 429:780–784.
28. Sansen S, De Ranter CJ, Gebruers K, Brijs K, Courtin CM, Delcour JA, Rabijns A. Structural basis for inhibition of *Aspergillus niger* xylanase by *Triticum aestivum* xylanase inhibitor-I. J Biol Chem 2004;279:36022–36028.
29. Chelliah V, Blundell TL, Fernandez-Recio J. Efficient restraints for protein-protein docking by comparison of observed amino acid substitution patterns with those predicted from local environment. J Mol Biol 2006;357:1669–1682.
30. Eghiaian F, Grosclaude J, Lesceu S, Debey P, Doublet B, Treguer E, Rezaei H, Knossow M. Insight into the PrPC–>PrPSc conversion from the structures of antibody-bound ovine prion scrapie-susceptibility variants. Proc Natl Acad Sci USA 2004; 101:10254–10259.